Master's Thesis

Phase Engineering of Two-dimensional Transition Metal Dichalcogenides for Electrocatalyst Application

Sanghyeon Park

Department of Energy Engineering

(Energy Engineering)

Graduate School of UNIST

2020

Phase Engineering of Two-dimensional Transition Metal Dichalcogenides for Electrocatalyst Application

Sanghyeon Park

Department of Energy Engineering
(Energy Engineering)

Graduate School of UNIST

Phase Engineering of Two-dimensional Transition Metal Dichalcogenides for Electrocatalyst Application

A thesis/dissertation
submitted to the Graduate School of UNIST
in partial fulfillment of the
requirements for the degree of
Master of Science

Sanghyeon Park

01/10/2020 of submission
Approved by

_____

Advisor
Hyesung Park

Phase Engineering of Two-dimensional Transition Metal Dichalcogenides for Electrocatalyst Application

Sanghyeon Park

This certifies that the thesis/dissertation of Sanghyeon Park is approved.

01/10/2020

signature

_____

Advisor: Hyesung Park

signature

_____

Jungki Ryu

signature

_____

Jun Hee Lee

Abstract

Two Dimensional (2D) materials such as transition metal chalcogenides (TMDs) has been studied, but several problems still remain as disturbance for application to energy materials like electrocatalyst. In this work, we present a phase engineering of TMDs for electrocatalyst via highly reactive molten Potassium (K) metal intercalation. The 2H to 1T phase transition of TMDs has been exploited for application of the 1T phase with metallic property to applications such as electrocatalysts. However, the improving stability of thermodynamically metastable 1T TMDs remains an important challenge to overcome for using 1T phase properties. In addition, scalable synthesis methods of 1T TMDs, which are necessary for a wide range of applications, have to be developed. In this work, we presented a synthesis method of 1T phase MoS_2 using molten K metal intercalation suitable for scalable method and confirmed the sucessfully phase transition 2H to 1T phase and improvement of 1T phase stability by K atom doping in the MoS_2 basal plane. Furthermore, K atoms are doped in MoS_2 basal plane, which can donate electron continuously to MoS_2, which achieved long-term stability, thermal stability, and high power laser stability. Furthermore, we applied K doped 1T MoS_2 to the hydrogen evolution reaction (HER) electrocatalyst and confirmed the improved HER performance owing to high electrical conductivity and basal plane activation of K-doped 1T MoS_2 compared to 2H MoS_2 and 1T MoS_2 (n-BuLi), and high phase stability of K-doped 1T MoS_2 exhibits high HER stability.

Contents

List of Tables

List of Figures

Figure 1.10. (a) Atomic force microscopy (AFM) of K doped 1T MoS_2 on SiO_2 substrate. (b) Thickness distribution of 100 flakes based on AFM images.

Figure 1.11. Analysis of phase stability of K doped 1T MoS_2. (a-b) XPS spectra of K doped 1T MoS_2 with increased annealing temperature. (a) Mo 3d (b) K 2p scan (c-d) Raman and UV-vis spectra of K doped 1T MoS_2 with increasing annealing temperature.

Figure 1.12. (a) 1T and 2H phase ratio depending on annealing temperature (b) TGA and DSC analysis in air atmosphere of K-doped 1T MoS_2 showing the K-doped 1T MoS_2 conversion to 2H phase at 350 °C.

Figure 1.13. (a) HRTEM image of K doped 1T MoS_2 after stored in air for 300 days. (b) 1T phase region of the enclosed by the blue square in (a). (c) Atomic arrangement of 2H phase region of the enclosed by the red square in (a). This show that 1T phase remains more dominant than 2H phase after 300 days.

Figure 1.14. (a) Raman spectra (b) UV-vis spectra of K doped 1T MoS_2 after stored in air for 300 days.

Figure 1.15. Raman spectra of (a) K doped 1T MoS_2 and (b) 1T MoS_2 (n-BuLi) after irradiation by a 532 nm laser source for 10 minute. When irradiated with a 532 nm laser, the 1T MoS_2 synthesized by n-BuLi is easily converted to the 2H phase.

Figure 1.16. XPS spectra of 1T MoS_2 synthesized by using n-BuLi. The 1T phase ratio determined from the XPS results is ~ 75%.

Figure 1.17. HER catalyst application (a, d) Linear sweep voltammetry (LSV) curves in (a) 0.5 M H_2SO_4 (d) 1 M KOH aqueous solution. (b, e) Corresponding Tafel slope for K doped 1T MoS_2, 1T MoS_2 (n-BuLi), 2H MoS_2, and Pt/C. (c, f) Electrochemical impedance spectroscopy of HER in (c) 0.5 M H_2SO_4 (f) 1 M KOH. (g) Electrochemical double layer capacitance of K doped 1T MoS_2, 1T MoS_2 (n-BuLi), and 2H MoS_2 obtained from CV. (h–i) CV cyclic stability profiles of K-doped 1T-MoS2 in (h) 0.5 M H_2SO_4, (i) 1 M KOH aqueous solution. Inset: Time dependent profiles of HER current density on K doped 1T MoS_2 at the overpotential.

Figure 1.18. Cyclic voltammetric (CV) curves for (a) K doped 1T MoS_2, (b) 1T MoS_2 (n-BuLi), (c) 2H MoS_2

Figure 1.19. Turn over frequency (TOF) plots for the HER of K doped 1T MoS_2, 1T MoS_2 (n-BuLi), and 2H MoS_2.

1. Synthesis of 1T MoS_2 via molten Potassium metal intercalation and doping

1.1 Research background

Transition metal dichalcogenides (TMD) is a typical 2-dimensinal material composed of an X-M-X layer laminated by a Van der Waals interaction. Polymorphs of MX_2 compounds such as MoS_2 and WS_2 are present in 1T and 2H phase based on coordination of M and X atom[1-2]. As shown in Figure 1.1, 2H phase has MS_6 trigonal coordination and consists of two S-M-S layers. 2H MoS_2 has a semiconductor characteristic with a band gap of about 1.2 eV[3-5]. On the other hand, 1T MoS_2 is composed of one S-M-S layer with MS_6 octahedral coordination and has a high electrical conductivity due to its metallic property as opposed to the 2H-phase having semiconductor characteristics, which is attributed to the electron density in valence *d* orbitals of transition metal[6-7], so 1T phase MoS_2 is applied to various electronic devices such as battery[8-11], hydrogen evolution catalyst[12-16], and supercapacitor[6, 17-20].

Depending on the electron fling in the d orblital of metal atoms, MoS_2 appears in different polyporph phase, including 3R (three layers of elongated cotton multi-shape and Mo atom in 3 angled prism adjustment), 2H (two layers of six square and three square prism adjustment Mo) and 1T (triangle with one layer and an octahedral adjusted Mo atom) representing various optical and electronic characteristics. The 3R phase of MoS_2 with the least studied demonstrates the potential for functional integrated photons due to their inherent special nonlinear behavior. The bulk 2H MoS_2 indirect band gap on the single layer 2H MoS_2. In contrast, 1T-MoS_2 is hydrophilic and metallic. Thus, in the field of electrochemical reaction and energy storage, the resistance to transmission of charge is reduced rapidly to 1T MoS_2, providing much better performance for the 1T phase of MoS_2 Moreover, the magnetic properties of MoS_2 can be significantly improved as the crystal structure is converted from 2H to 1T. Metal and translucent 1T MoS_2 offers new opportunities for transparent conductor development.

However, in thermodynamic perspective, the phase of MoS_2 is more stable and preferred in 2H phase, so the metastable 1T phase does not exist in nature[21-22]. To synthesize 1T phase MoS_2, various methods for 2H-to-1T phase transition of TMDs including intercalation with alkali metal[7, 23-24] and electron donor materials (ammonium[25], phosphorus[26]), electron beam irradiation[27], and mechanical strain[28,29] have been proposed. Among them, n-Butyllithium intercalation (chemical exfoliation) is still the most widely used strategy to synthesize the 1T-TMDs. However, the chemical exfoliation is complex and inadequate for complete phase transition with high-purity, because n-Butyllithium (n-BuLi) tends to form relatively large molecules of dimeric or trimeric structures, which diffuse slowly into the interlayer of TMDs. However, the synthesized 1T MoS_2 is not suitable for mass production due to its very long synthesis time[30] and low yield[31], and thermal stability is also low, so it has the disadvantage that the characteristics of 1T phase are easily lost and converted to 2H phase when applying energy device[32, 33]. Furthermore, a fatal drawback is that when the electron donor is completely removed from

the surface of the TMDs via post treatments, 1T phase is easily converted to 2H phase, which severely restricts using electrical conductivity and catalytic activity of the 1T phase TMDs.

Therefore, the synthesis method that can maintain highly stable 1T phase MoS_2 remains big challenge. The method of lattice mismatch[34], electron donor atom doping was proposed. Intercalation or doping of a material having a lone pair electron such as alkali metal[25-26] can lower the activation energy to convert 1T to 2H, thereby maintaining 1T phase more stable than 2H phase. In addition, metal doping can maintain the octahedral coordination by trapping the sulfur site of 1T phase, and can maintain the Mo 3*d* orbital electronic structure of 1T phase by continuously electron transfer to Mo atom through doping of atom with lone pair electron[35,36]. Although density functional theory (DFT) confirmed that the formation energy of the 1T phase is more stable than the 2H phase via electron donor doping in previous studies, typical electron donor doping methods for improving the 1T phase stability through generally requires harsh conditions such as the use of toxic gas, and chemical vapor deposition (CVD) process at high pressure and temperatures.[37] Therefore, comparatively facile method that easily electron donor doped to the TMDs basal plane is indispensable to take full advantage of the properties of stable 1T-TMDs.

In this work, we propose a molten potassium metal intercalation and doping method that is more reactive than alkali ions for the synthesis of 1T MoS_2. K doped 1T MoS_2 synthesized through the proposed synthesis method has 1T phase of up to 92% and 1T MoS_2 synthesis with 80% yield. In addition, it was confirmed by calculation that the 1T phase is more stable than the 2H phase by K atom doping, which acts as an electron donor. It was confirmed that the synthesized K doped 1T MoS_2 maintains the 1T phase stably for 300 ° C, air atmosphere, and 532 nm laser. In addition, by applying K doped 1T MoS_2 having high phase purity and phase stability to the hydrogen generating catalyst, HER efficiency and stability were improved compared to 1T MoS_2 and 2H MoS_2 synthesized using n-BuLi.

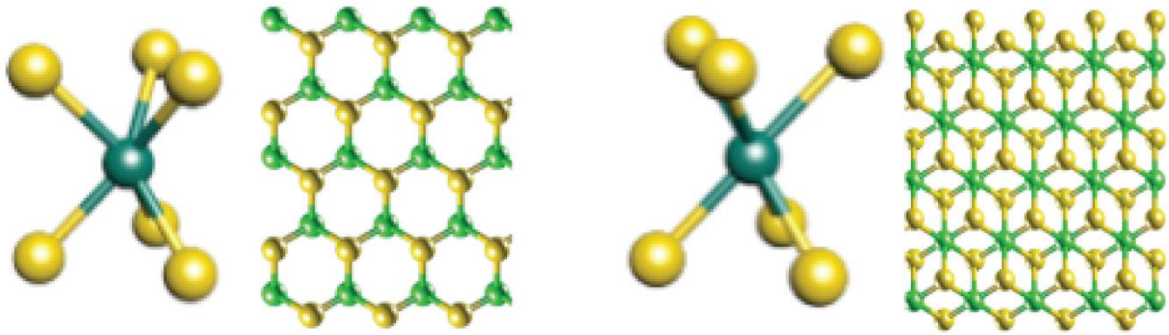

Figure 1.1. Atomic and lattice structure of 2H and 1T phase MoS_2.

1.2 Experimental section

1.2.1 Synthesis of K-doped 1T-MoS_2

For the synthesis of K-doped 1T-MoS_2, 500 mg of bulk MoS_2 powder (<2 μm, purity >98%, Sigma-Aldrich) and 200 mg of potassium metal (stored in oil, purity>99.95%, Kojundo Korea) were filled in glass tube under nitrogen atmosphere. The set of tubes was sealed through a vacuum line and treated at 400 ℃ for 1 h. Obtained K_XMoS_2 dispersion in deionized water (10 mg/mL) was exfoliated via mild sonication (CPX2800H, Branson) for 1 h. To remove the unexfoliated MoS_2, centrifugation (VARISPIN 15R, CRYSTE) was performed at 3000 rpm for 30 min. The resulting suspension was filtered and washed using isopropyl alcohol and ethanol to remove potassium ion residues. Filtrated K-doped 1T-MoS_2 powder was dried at 70 ℃ for 6 h.

1.2.3 Synthesis K-doped 1T-WS_2

The synthesis method is similar to the synthesis of K-doped 1T-MoS_2, but WS_2 powder (<2 μm, purity >99%, Sigma-Aldrich) was used as the TMDs.

1.2.4 Synthesis K-doped 1T-$MoSe_2$

The synthesis method is similar to the synthesis of K-doped 1T-MoS_2, but $MoSe_2$ powder (purity >99.9%, Alfa Aesar) was used as the TMDs.

1.2.2 Synthesis of 1T MoS_2 (chemical exfoliation)

Lithium intercalation was done in an Ar-filled flask. The intercalation of 500 mg MoS_2 (Sigma-Aldrich) was carried out by stirring (1200 rpm) in BuLi/hexane solution (30 mL, 5 M, Sigma-Aldrich) in a 50 mL 2 neck round bottom flask for ~48 h. After intercalation, excess BuLi was recovered by filtration and washing with hexane. Ther Li intercalated MoS_2 was exfoliated by sonication (135 W, Branson 2800). and the intercalated samples were retrieved by centrifugation and washed three times with 40 mL of hexane to remove excess lithium and organic residues. 1T MoS_2 in DI water dispersion was washed through 12,000 rpm centrifuge (CRYSTE, VARISPIN 12).

1.2.3 Material characterizations

Structural characterizations were conducted by High-power XRD (D/MAX2500V/PC, Rigaku) at a scan rate of 1 ° min^{-1}. The absorption of 2H-MoS_2 and K-doped 1T-MoS_2 dispersion were measured through UV-vis-NIR spectrophotometer (Cary 5000, Agilent). Raman and photoluminescence spectra were obtained with confocal Raman (alpha300R, WITec) using a 532 nm laser. Sheet resistance for calculate electrical conductivity was measured by 4-point probe (CMT-SR2000N, Advanced Instrument Technology). Chemical composition and changing the oxidation state were carried out by

XPS measurement (ESCALAB 250XI, Thermo Fisher Scientific). Morphological characterizations was conducted using Dimension AFM (DI-3100, Veeco) and HR-TEM (JEM-2100F, JEOL). EDS elemental mapping was carried out using JEOL 21000F microscope at voltage of 200 kV. Thermal analysis for confirmation of phase conversion was conducted using TGA (Q500, TA) and DSC (Q200, TA) at a scan rate 5 ℃ min^{-1}.

1.2.4 Electrochemical characterization

The electrochemical reduction profiles of rotating disk electrode (RDE) were measured by depositing thin film of catalysts by preparing the catalyst ink on the glassy carbon disk electrode, where area is 0.1256 cm^2. Each catalyst was prepared in the form of an ink by dispersing 18 mg of the catalyst and 2 mg of Ketjen Black (EC-600JD) in 1 mL of a binder solution followed by a bath sonication process, where the binder solution is prepared by mixing ethanol, isopropyl alcohol, and 5 wt.% Nafion solution (Sigma-Aldrich) with a volumetric ratio of 45:45:10. A platinum wire was used as a counter electrode and Ag/AgCl (saturated KCl filled) was used as a reference electrode. An aqueous solution of N_2-saturated 0.5 M H_2SO_4 and 1 M KOH were used as the electrolyte. The electrochemical tests were carried out using a computer controlled potentiostat (Biologic VMP3) with an RRDE-3A (ALS Co.) rotating disk electrode system at a scan rate of 10 mV sec^{-1}. A calibration in reversible hydrogen electrode (RHE) was experimentally determined at a scan rate of 1 mV s^{-1}, in H_2-saturated 0.5 M H_2SO_4 and 1 M KOH where platinum wire was used as the working and counter electrode and Ag/AgCl as the reference electrode. For all half-cell configured experiments, iR drops were compensated by measuring the resistance of solution under the working condition.

1.3 Synthesis mechanism of K doped 1T MoS_2

K-doped 1T MoS_2 is synthesized by MMI method, as illustrated in Figure 1.1. A glass tube (6 mm in diameter) filled with bulk MoS_2 powder (500 mg) and potassium metal (200 mg) was inserted in a larger glass tube (10 mm in diameter). While reacting at 400 ℃ for 1 hour, the MoS_2 powder is impregnated through the capillary action of molten potassium metal and the potassium molecules are spontaneously intercalated into the MoS_2 interlayers by the potential gap between electron affinity of MoS_2 (4.45 eV) and ionization potential of potassium (4.34 eV) [37, 38]. The low ionization potential of potassium easily donates the electron in reaction with MoS_2, simultaneously MoS_2 easily accept electrons from the potassium owing to the high electron affinity of MoS_2. Furthermore, the some of the intercalated K atoms forms the ionic bonding with more electronegative S atom

than Mo atom. The reason for the K–S ionic bonding is that the difference in electronegativity between K atom and S atom is 1.76, therefore the electron can be transferred from K atom to the MoS_2. As a result, 300 mg of K-doped 1T MoS_2 powder can be synthesized via MMI method. The digital image shown in Figure 1.2 is the K-doped 1T MoS_2 dispersed in deionized water with concentration of 1 mg/mL, demonstrating that gram scale synthesis of K-doped 1T MoS_2 is possible. Notably, the general applicability of the MMI method has also been validated as an expandable method to apply phase engineering of other VI-TMDs, WS_2 (Figure 1.3).

1.4 Characterization anlaysis of K doped 1T MoS_2

The XRD anlyasis was performed to confirm MoS_2 exfoliation and molten Potassium metal intercalation. As shown in Figure 1.4 a,b, as the exfoliation of bulk MoS_2, the intensity of the (002) peak near 14 ° was reduced, but it was confirmed that the sharp peak was still maintained and the crystallinity was maintained. In particular, there is no peak exept for the XRD peak of MoS_2. This suggests that Potassium was mainly doped in the plane of MoS_2 rather than in the formation of new compouds. Figure 1.4 b show the intensity of the (002) peaks is reduced and shift toward smaller angle. In case of K_xMoS_2 (K c/2 = 8.99 Å), the main peak appears at 11.4 °. This is a value shifted by about 3 ° compared to bulk MoS_2, which means that the interlayer distance of MoS_2 (002) plane is widened by K atom according to Bragg's law. [39, 40] Such blue shift in K_xMoS_2 suggests the increased MoS_2 interlayer spacing in the K_xMoS_2 from 6.1 Å to 7.7 Å owing to spontaneous K atom intercalation via MMI method. And the sharp (002) plane XRD peak of K-doped 1T-MoS_2 presented considerably decreased intensity compare to the that of bulk MoS_2, indicating that the K-doped 1T-MoS_2 with high planar crystal structure are successfully exfoliated. Even after the exfoliation the (002) plane of K doped 1T MoS_2 is observed with a blue shift of 0.5° (13.9°) relative to bulk MoS_2 and 2H MoS_2 nanosheets, suggesting that the MMI method using highly reactive molten potassium not only efficiently intercalated between the MoS_2 interlayer, but also doped K atom in MoS_2 basal plane.

As the transition from the 2H phase to the 1T phase, the big difference characteristic is change the electrical conductivity. Also, to prove this, the electrical conductivity was compared by using 4 point probe. Clearly, the K doped 1T MoS_2 has a significantly higher electrical conductivity of 8723 S/m compared to 2H MoS_2, which is about 330 times higher than 26.5 S/m of 2H MoS_2. As shown in Figure 1.2 d, the J_1, J_2, and J_3 phonon modes are due to the 1T phase S-Mo-S, which clearly indicates that the phase is converted from 2H to 1T phase. In Raman spectrum of 2H MoS_2, two main Raman modes can be identified at 383 cm^{-1} (E^1_{2g} mode) and 401 cm^{-1} (A_{1g} mode), arising from the in-plane and out-of-plane vibration modes of MoS_2, respectively. Meanwhile, K doped 1T MoS_2 exhibits seven Raman mode peaks at 383 cm^{-1} (E^1_{2g} mode, which suggests structural symmetry of 1T phase lattice), 401 cm^{-1} (A_{1g} mode), 280 cm^{-1} (E_{1g} mode, which is attributed to the octahedral coordination of Mo), 152 cm^{-1} (J_1

mode), 201 cm^{-1} (J_2 mode), 337 cm^{-1} (J_3 mode), and 240 cm^{-1} (K–S out-of-plane stretching Raman mode, which is attributed to K atom doping on MoS_2 basal plane). The J_1, J_2, and J_3 peaks in the Raman spectra of K doped 1T MoS_2 are attributed to a longitudinal acoustic phonon modes of 1T phase.The presence of this feature is due to the zone-folding mechanism due to the formation of a superlattice in the base plane of the 1T MoS_2. Also, the A_{1g} (out-of-plane vibration) to E^1_{2g} (in-plane vibration) reflects means Mo-S stretching of MoS_2. In addition, the peak formed at 240 cm^{-1} corresponds to the out of plane stretching of K-S bonding. The photoluminescence (PL) spectra of K doped 1T MoS_2 and 2H MoS_2 flakes are demonstrated in Figure 1.4e. As shown in Figure 1.4f, phase conversion of MoS_2 investigated by ultraviolet-visible absoroption spectrum. As the phase changed from 2H to 1T phase, the A and B exciton peaks due to the semiconducting properties disappear and the metallic behavior is shown.[41] UV-vis-NIR (UV-vis-NIR) absorption spectra of 2H MoS_2 and K doped 1T MoS_2, which demonstrate the semiconducting feature of 2H MoS_2 with A and B excitonic peaks at ~675 and ~612 nm corresponded to direct excitonic transition from valence band to the conduction band. On the other hand, K-doped 1T-MoS_2 shows the featureless spectrum with suppression of two excitonic peaks, indicating that the MMI method can successfully transform of the 2H phase (semiconducting) to the 1T phase (metallic).

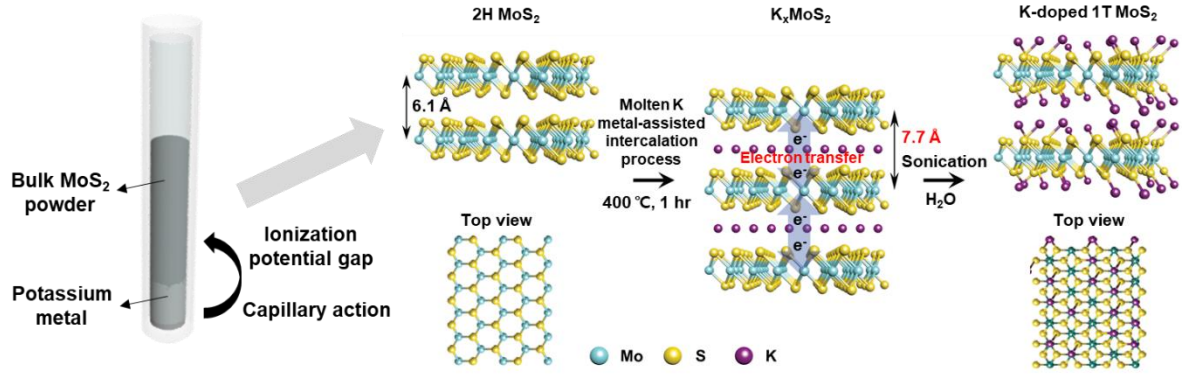

Figure 1.2. Schematic of synthesis of K doped 1T MoS_2 via molten potassium intercalation.

The XPS survey as shown in Figure 1.4g, h, i, shows that there are Mo 3d, S 2p, and K 2p in the case of K doped 1T MoS_2. The Mo 3d peaks of K doped 1T MoS_2 represented at 228.1 and 231.4 eV correspond to $3d_{5/2}$ and $3d_{3/2}$. On the other hand, Mo 3d peaks of 2H MoS_2 are found at 228.9 and 232.2 eV as high as 0.8 eV. The presence of the new peaks of K doped 1T MoS_2 results from the Fermi level shift because extra electrons are filled in the d orbits during the phase conversion process. In addition, 1T phase ratio was calculated based on XPS, and it was confirmed that 1T phase MoS_2 having high phase purity of about 92% was synthesized. The S 2p peak also represent new peaks are found. The S 2p peak of K doped 1T MoS_2. Accordingly, apart from the S $2p_{3/2}$ peaks of S $2p_{1/2}$ and 2H MoS_2 in the S 2p scan spectra, two new S 2p peaks were found, which further demonstrates the presence of 1T phase.

K doping of K doped 1T MoS_2 was confirmed by XPS K 2p scan. K 2p scans were seen at 295.9 and 293.2 eV, which is at K $2p_{1/2}$ and K $2p_{3/2}$, respectively. This results suggest that the K atoms can successfully donate the electron to MoS_2 through MMI method. Furthermore, the phase composition of K-doped 1T-MoS_2 was confirmed to 92.3% for 1T phase and 7.7% for 2H phase via XPS results, indicating that the K-doped 1T-MoS_2 synthesized by MMI method has high 1T phase purity. The binding energy showing the K 2p peak is formed by K-S covalent bonding and is consistent with the Raman spectra results. [6, 21]

In addition, as the phase changes, the hydrophilicity changes. In Figure 1.5, the water contact angles of K doped 1T MoS_2 and 2H MoS_2 are shown. 2H MoS_2 is hydrophobic in contact with water at 95.3°. On the other hand, K doped 1T MoS_2 can be seen to change to hydrophilic properties at 14.4 °. When applied to the electrocatalyst, this area maximizes the adsorption area with the aqueous electrolyte and facilitates hydrogen adsorption. Therefore, the hydrophilic properties of K doped 1T MoS_2 can be evidence of further improvement of electrochemical performance.[26]

Figure 1.3. Digital image of K doped 1T MoS_2 dispersion in DI water, which indicates that scalable synthesis of K-doped 1T MoS_2 is possible.

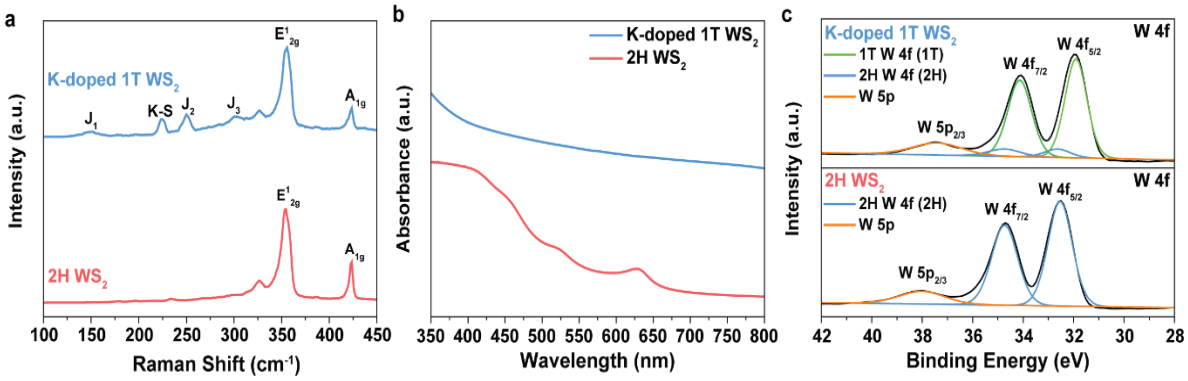

Figure 1.4. Comparison of of K doped 1T WS_2 synthesized by molten potassium intercalation and 2H WS_2 (a) Raman (b) UV-vis spectra (c) XPS spectra.

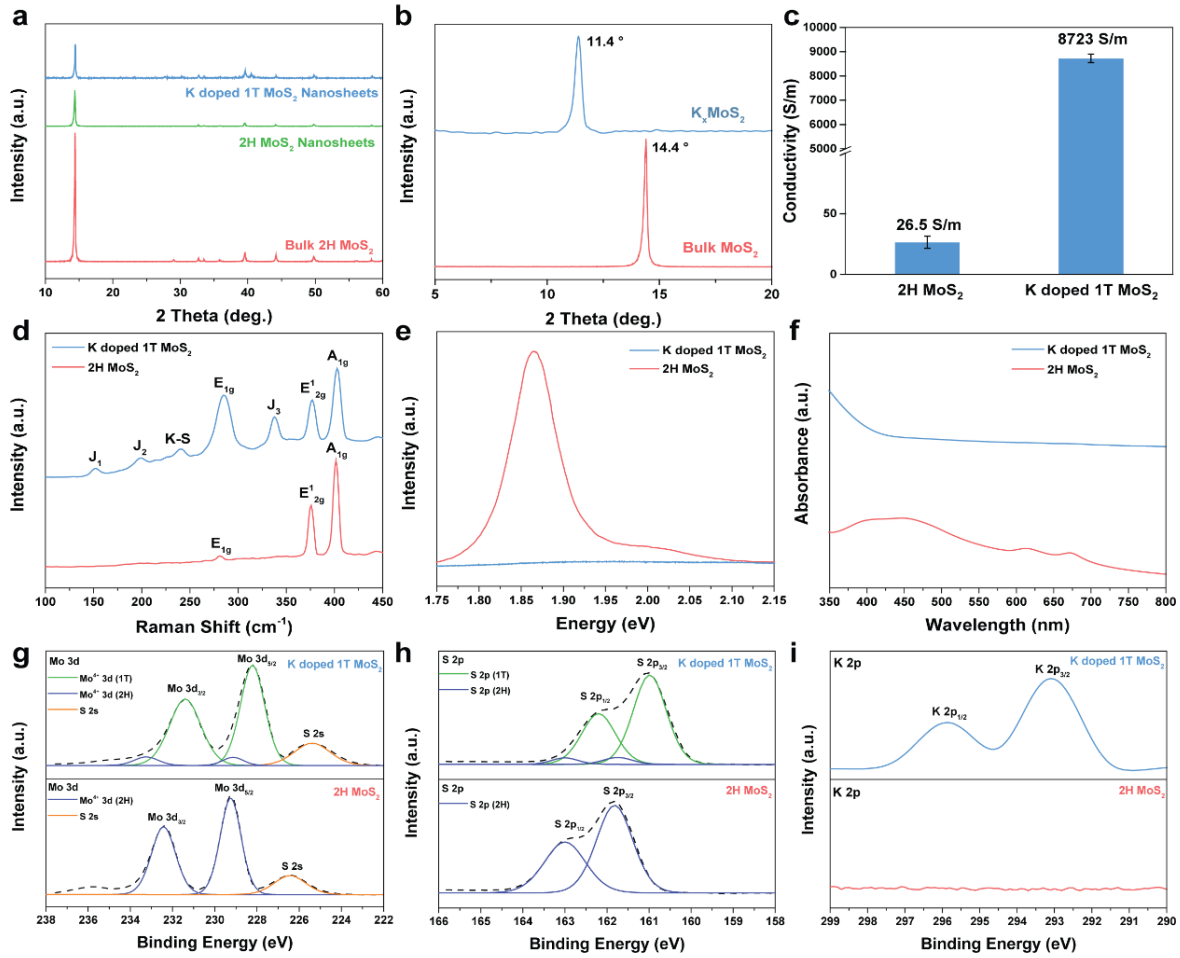

Figure 1.5. Comparison of characterization between K doped 1T MoS_2 and 2H MoS_2. (a) XRD patterns of K doped 1T MoS_2 compared with bulk 2H MoS_2 and nanosheets, and K doped 1T MoS_2. (b) Selected region of XRD patterns of K_xMoS_2 shows a clear shift of 2 theta which means the change of interlayer distance due to K ion intercalation. (c) Electrical conductivity using four-point probe of K doped 1T MoS_2 compared with 2H MoS_2 nanosheets. (d) Raman spectroscopy for K doped 1T MoS_2 and 2H MoS_2, showing the specific peaks of 1T phase MoS_2. (e) Photoluminescence spectroscopy of an as exfoliated 2H MoS_2 and K doped 1T MoS_2. (f) UV-vis spectra for 1T MoS_2 and 2H MoS_2. The PL and UV-vis results show that the A and B exciton peak in case of the K doped 1T MoS_2 are quenched. (g-i) Comparison of XPS spectra for K doped 1T MoS_2 and 2H MoS_2 (g) Mo 3d (h) S 2p (i) K 2p scan.

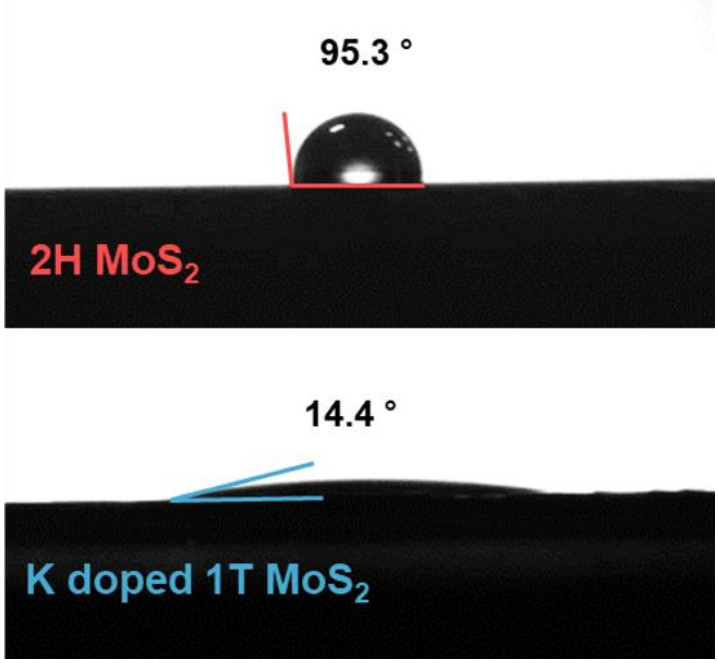

Figure 1.6. Contact angle of water droplets on the surface of K doped 1T MoS_2 and 2H MoS_2, respectively.

1.5 Morphological Chracterization of K doped 1T MoS_2

As shown in Figure 1.7, in order to investigate the morphology, microstructure and elemental mapping of the K doped 1T MoS_2 abtained high resolution transmission electron microscopy (HRTEM) was performed. Figure 1.7 a,b,c shows typical HRTEM images of K doped 1T MoS_2. In the K doped 1T MoS_2 sample, the lattice structure of 2H phase in red region (semiconducting, trigonal) and 1T phase in blue region (metallic, octahetral) were observed simultaneously. The 1T phase MoS_2 region showed a octahetral Mo-S atomic arrangement with interlayer distance of 0.27 nm, corresponding (100) plane of MoS_2. Clear lattice structure can be observed in the zoomed-in images of 1T and 2H phase.The 1T phase region showed the clear Mo–S octahedral coordination with lattice spacing of 0.27 nm, corresponding to the (100) plane of MoS_2. In contrast, 2H phase region showed typical Mo-S trigonal prismatic coordination. In addition, HRTEM images of synthesis temperature are shown in figure 1.8 (100, 200, 300 and 400 °C). When the synthesis temperature reached 400 °C, the ratio of 1T phase showed the highest ratio of 92.4% through HRTEM image, and it was confirmed that K atom is an optimization condition that intercalates between MoS_2 layers. The Mo-Mo interatomic arrangement of the K doped 1T MoS_2 lattice structure can be clearly observed at the light intensity shown in Figure 1.7d, along with a schematic. Mo-S-S-Mo atomic arrangement is shown in the 1T phase, while Mo-S-Mo atomic arrangement is observed in the 2H phase. This can be confirmed once more by phase

conversion. The energy dispersive spectrometry (EDS) mapping results show K doping and match the XPS and Raman spectra results in Figure 1.4 d,i. This shows a uniform element distribution of Mo (blue), S (yellow) and K (purple). As shown in figure 1.9 and Table 1.1, the atomic ratio obtained from the EDS mapping spectrum confirms that K is about 15% doped. In Figure 1.7 f shows the selected area electron diffraction (SAED) pattern of K doped 1T MoS_2 viewed along the (100) zone axis. In addition, one Mo atom is surrounded by six nearest neighboring Mo atoms, which is direct evidence of 1T phase. It also shows a high crystalline structure corresponding to the (100) plane of K doped 1T MoS_2 with a lattice spacing of 0.27 nm, which is consistent with XRD results.[42,43] In brief, the high 1T phase purity (>92%) and high crystallinity of K-doped 1T-MoS_2 can be attributed to the MMI method. By analyzing thickness of AFM image in Figure 1.10, we verified the thickness histogram of K doped 1T MoS_2 and most flakes are 2.52 nm (1-2 layers). The histogram was obtained from counting more than 100 flakes.

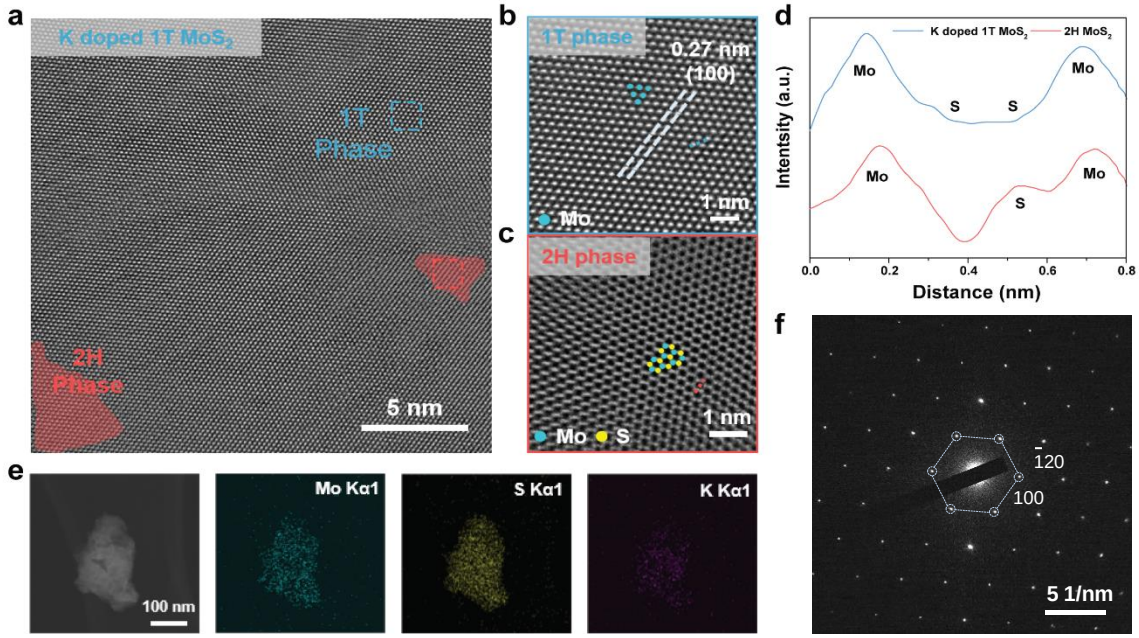

Figure 1.7. HRTEM analysis of K doped 1T MoS_2. (a) HRTEM image of K doped 1T MoS_2 showing both the dominant 1T and 2H phases of MoS_2. (b) Atomic arrangement of 1T phase region of the enclosed by the blue square in (a). (c) Atomic arrangement of 2H phase region of the enclosed by the red square in (a). (c) Light intensity profile of the line marked in (b) and (c). (e) EDS mapping images taken from the K doped 1T MoS_2 flake, indicating homogeneous distribution of molybdenum, sulfur, and potassium (f) Selected area electron diffraction (SAED) pattern of K doped 1T MoS_2 nanosheet.

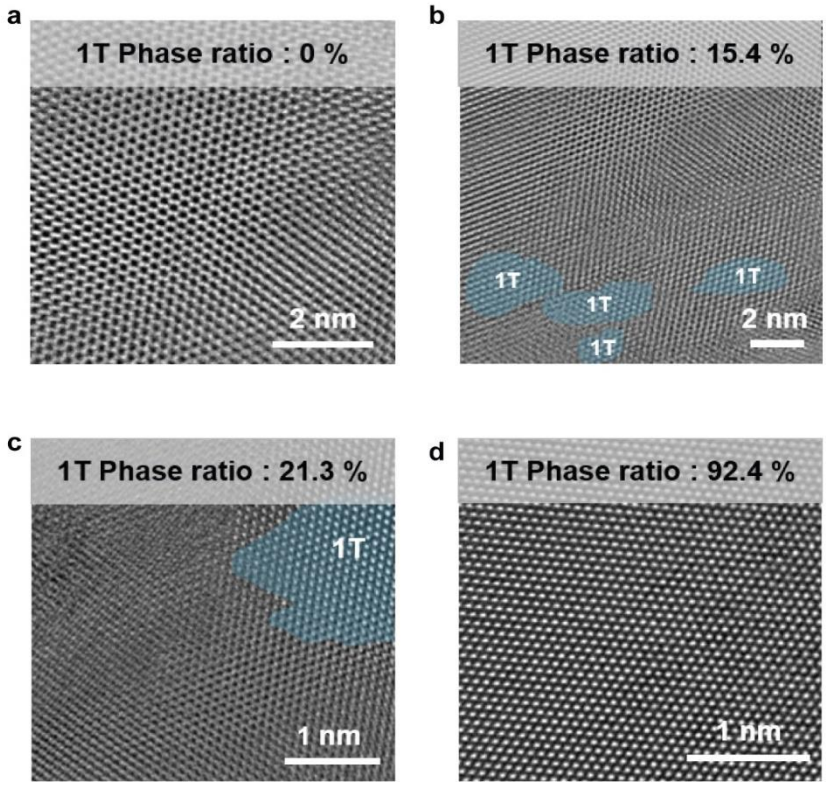

Figure 1.8. HRTEM images of synthesis at (a) 100 ℃, (b) 200 ℃, (c) 300 ℃, (d) 400 ℃ respectively, showing that 1T phase ratio changes with synthesis temperature

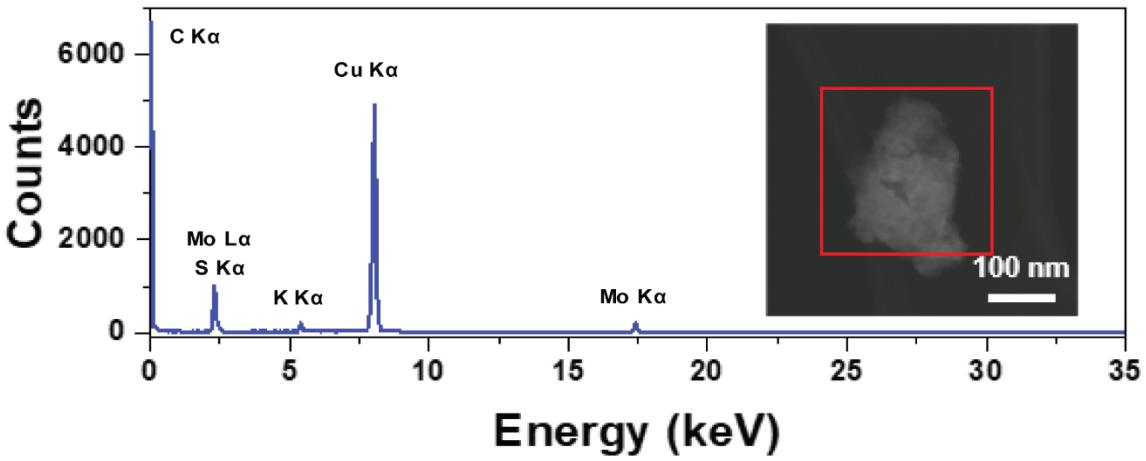

Figure 1.9. EDS mapping spectrum of K doped 1T MoS_2. The red rectangle in the inset image shows the selected EDS inspection field.

Element	Atomic %
Mo	**28.09**
S	**56.34**
K	**15.57**
Total:	**100.00**

Table 1.1. Element ratio of K doped 1T MoS_2 based on EDS mapping spectrum. The resulting spectrum and tabulated results show that K atoms are doped in non-oxidized MoS_2.

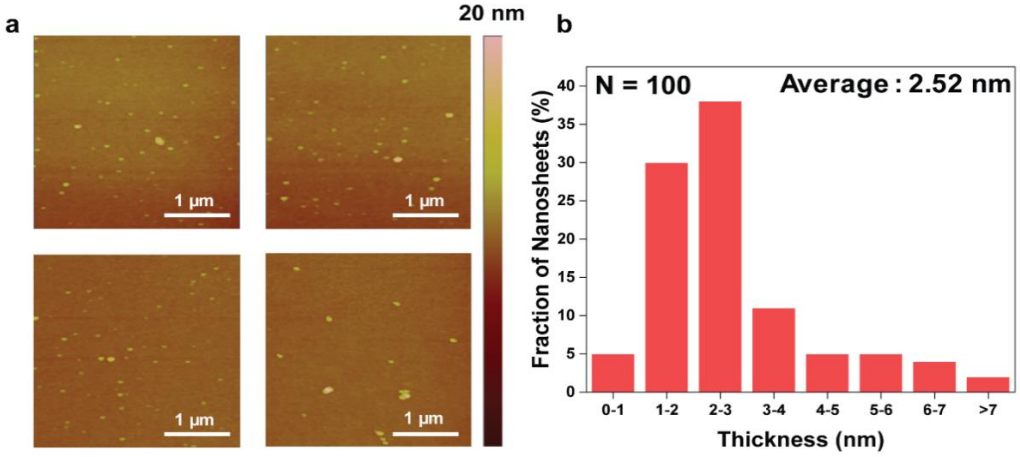

Figure 1.10. (a) Atomic force microscopy (AFM) of K doped 1T MoS_2 on SiO_2 substrate. (b) Thickness distribution of 100 flakes based on AFM images. The average thickness of K doped 1T MoS_2 is 2.52 nm.

1.6 Phase stability of K doped 1T MoS_2

In general, the biggest problem with 1T MoS_2 synthesized via n-BuLi intercalation is that the phase easily changes to a thermodynamically stable 2H phase. The reason for the low phase stability is that 2H phase is low energy and stable as the intercalated electron donor Li ion is removed.[44] Therefore, we analyzed whether phase stability of 1T phase MoS_2 improved as electron donor K atom was doped in in MoS_2 plane, was doped in Figure 1.11. First, K doped 1T MoS_2 sample was thermally annealed on hot plate in the air atmosphere for one hour and phase transition was investigated by using XPS Mo 3d and K 2p scan in Figure 1.11 a, b. The XPS Mo3d spectrum of the K doped 1T MoS_2 annealed at 100, 200, 300, and 350 ℃ is shown in Figure 1.11 a. XPS results suggested that the initial K doped 1T MoS_2 consisted of 92.3% 1T phase. As the annealing was introduced and the annealing temperature increased, the 1T fraction of K doped 1T MoS_2 consisting according to the 1T phase peak intensity only lost about 20% for the sample annealed at 300 °C. However, when annealing was performed at about 350 °C, the 1T phase fraction became 0% and completely changed to the 2H phase. This tended to be similar to XPS K2p scan shown in 1.11 b. K atom, which can give electrons to MoS_2 plane, also showed a clear peak at the beginning, but it was confirmed that no K-related peak appeared when the annealing temperature reached 350 °C. This proves that 1T phase conversion and 1T phase stability due to K atom doping can be improved. In addition, the high 1T phase stability was found to be dependent on the K atom doping on the MoS_2 nanosheets. Despite annealing at 300 °C, the 1T phase fraction was maintained to 74.7% by K atom doping. Raman and UV-vis specra also demonstrate 1T phase maintenance as shown in Figure 1.11 c,d. In Raman analysis, the peaks J_1, J_2, and J_3 due to the 1T phase were maintained at annealing temperatures up to 300 °C. On the other hand, at annealing temperature of 350 ℃, J_1, J_2, and J_3 peaks disappeared and only 2H phase-related peaks E_{1g}, E^1_{2g}, and A_{1g} peaks were observed. The UV-vis spectra also showed that when the annealing temperature reached 350 °C, the A and B exciton peaks formed and changed to semiconducting properties. In addition, the result of confirming the ratio of K doped 1T MoS_2 through XPS shows that it has a high thermal stability while maintaining the 1T phase ratio of 74.7% up to 300 °C (Figure 1.12 a).

Differential scanning calorimetry (DSC) and thermal gravimetric analysis (TGA) analyzes in air atmosphere are shown in Figure 1.11 b to confirm thermal phase conversion. DSC results show that K doped 1T MoS_2 has a weight loss of 2.6% due to chemically and physically adsorbed water on the K doped 1T MoS_2 surface up to 400 ℃. This means that there is no weight loss due to degradation of K doped 1T MoS_2. Strong exothermic peaks are observed around 350 ℃ on the DSC curve. In general, the reaction from 2H to 1T phase is exothermic, and the exothermic peak at 350 ℃ means conversion to 2H phase. In other words, as the K-S bonding is broken at 350 ℃ and the electron donor is removed, the transition from the 1T phase to the 2H phase is confirmed. This coincides with the results of Figure 1.12 and means ultrastable with 1T phase up to 300 ℃.[45] Interestingly, the K atomic percentage as

a function of the annealing temperature is commensurate to the 1T phase percentage with annealing temperature, demonstrating that continuous electron donating through K atomic doping is the main cause of phase transition and high phase-stability.

The stability of K doped 1T MoS_2 in air was also analyzed. After storage in air for 300 days, HRTEM images of K-doped 1T MoS_2 are shown in Figure 1.13 a. After 300 days in the air, the 1T phase remains more dominant than 2H phase. Enlarged HRTEM image in Figure 1.13 b, c shows typical HRTEM images of K doped 1T MoS_2. In the K doped 1T MoS_2 sample, the lattice structure of 2H phase in red region (semiconducting, trigonal) and 1T phase in blue region (metallic, octahetral) were observed simultaneously. After 300 days in air, Raman and UV-vis analysis, shown in Figure 1.14, of the K doped 1T MoS_2 were also investigated to confirm 1T phase maintenance. Raman analysis showed that the J_1, J_2, and J_3 peaks were still maintained, indicating the Raman peak of the 1T phase MoS_2. In addition, K-S bonding out-of-plane stretching peaks appearing at 240 cm^{-1} were also maintained and K atom doping was maintained. UV-vis analysis also revealed that the A and B exciton peaks did not appear and maintained the metallic 1T property. The phase conversion was also investigated by Raman spectroscopy in Figure 1.15. The Raman spectra show the difference in stability of K doped 1T MoS_2 and 1T MoS_2 synthesized using n-BuLi. The Raman spectra of K doped 1T MoS_2 in Figure 1.15 a shows the maintain of the 1T phase despite the 532 nm laser irradiation for 10 min. The phase transition of K doped 1T MoS_2 is ultrastable under irradiation by a 532 laser for 10 min. In contrast, the 1T MoS_2 synthesized using n-BuLi completely transitions to the 2H phase when irradiated with 532 nm laser for 30 seconds, as shown in Figure 1.15 b. Through the following analysis, it was confirmed that ultrastable K doped 1T MoS_2 maintains the 1T phase very well by K atom which is electron donor even in heat, atmosphere and strong laser.

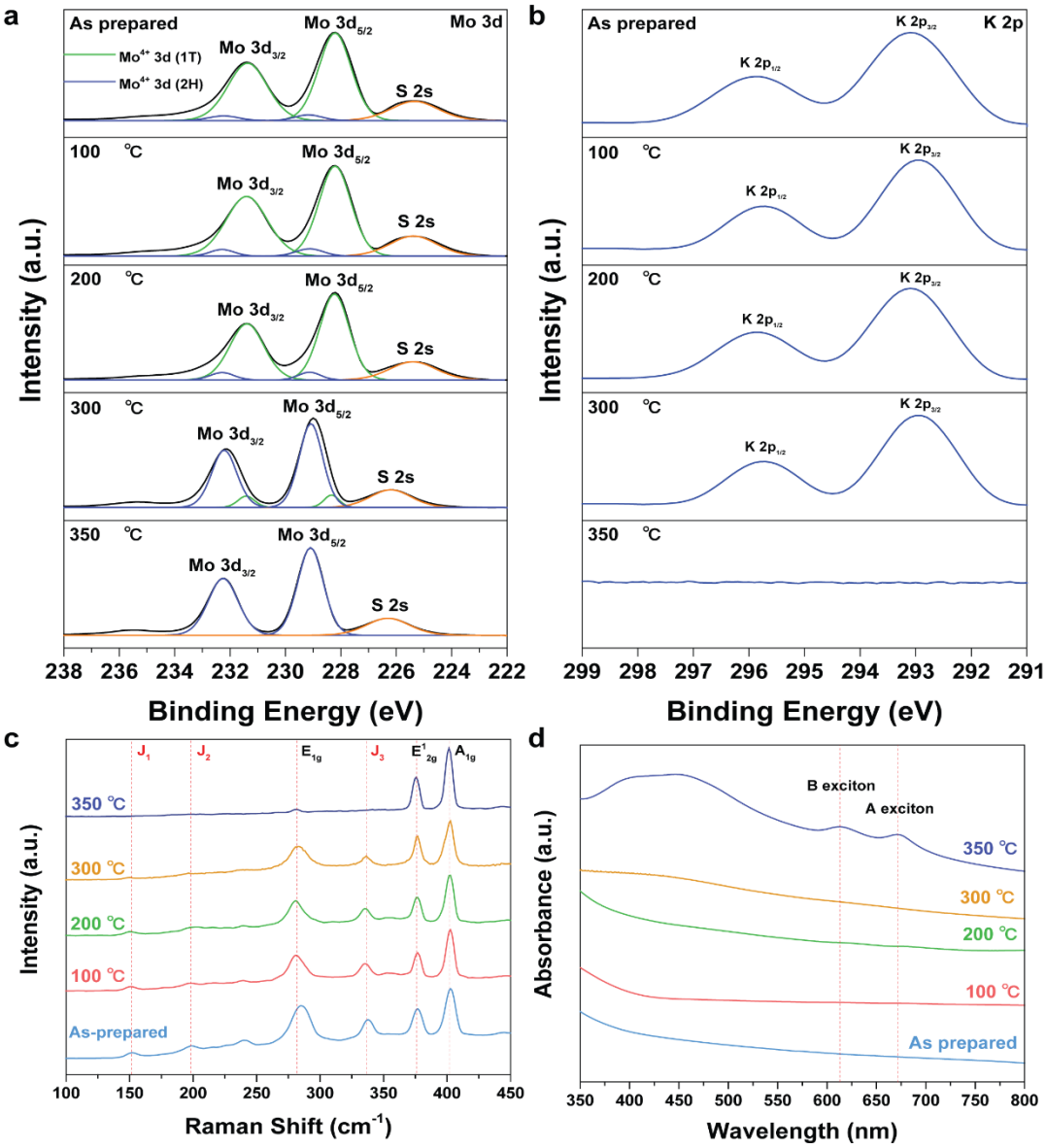

Figure 1.11. Analysis of phase stability of K doped 1T MoS_2. (a-b) XPS spectra of K doped 1T MoS_2 with increased annealing temperature. (a) Mo 3d (b) K 2p scan (c-d) Raman and UV-vis spectra of K doped 1T MoS_2 with increasing annealing temperature.

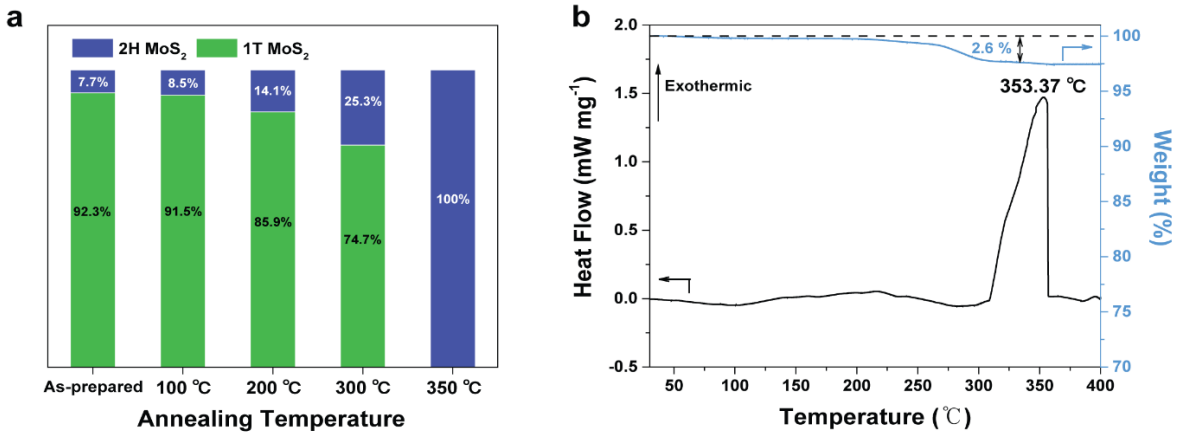

Figure 1.12. (a) 1T and 2H phase ratio depending on annealing temperature (b) TGA and DSC analysis in air atmosphere of K-doped 1T MoS_2 showing the K-doped 1T MoS_2 conversion to 2H phase at 350 ℃.

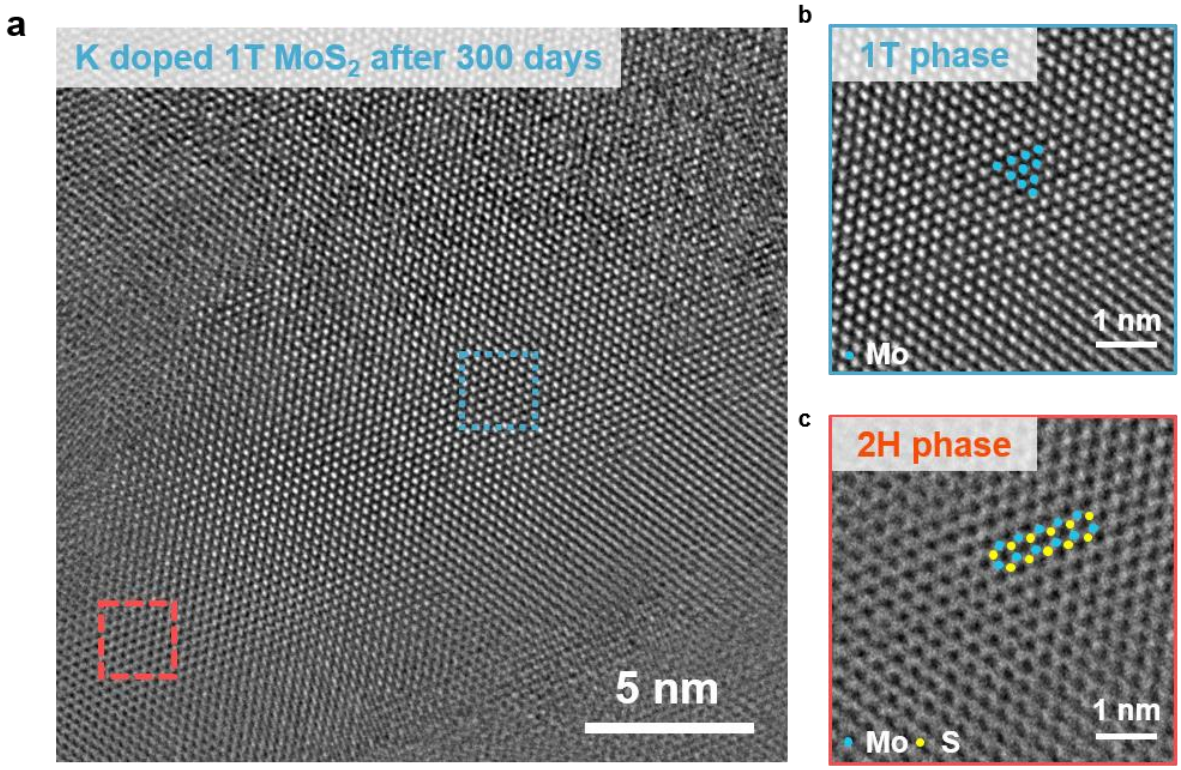

Figure 1.13. (a) HRTEM image of K doped 1T MoS_2 after stored in air for 300 days. (b) 1T phase region of the enclosed by the blue square in (a). (c) Atomic arrangement of 2H phase region of the enclosed by the red square in (a). This show that 1T phase remains more dominant than 2H phase after 300 days.

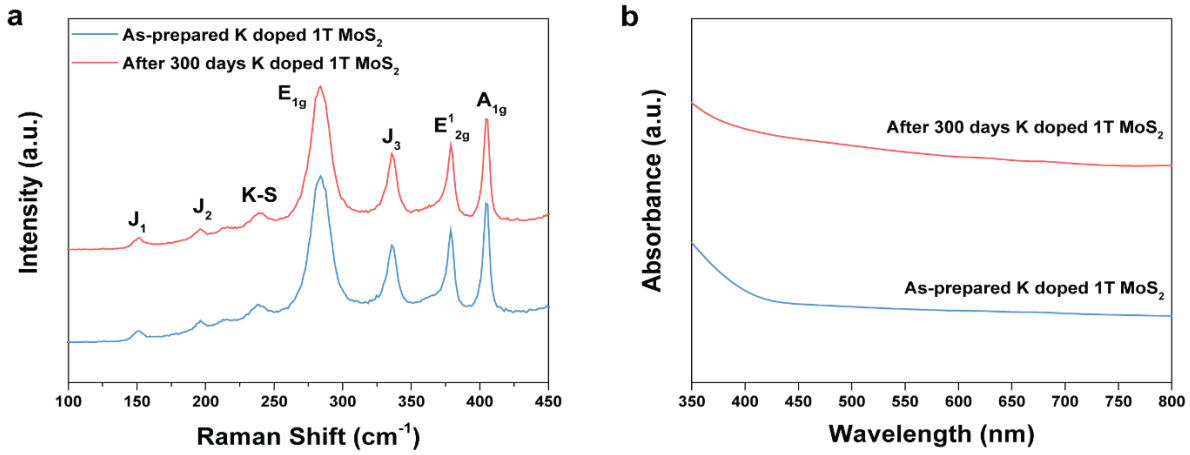

Figure 1.14. (a) Raman spectra (b) UV-vis spectra of K doped 1T MoS_2 after stored in air for 300 days.

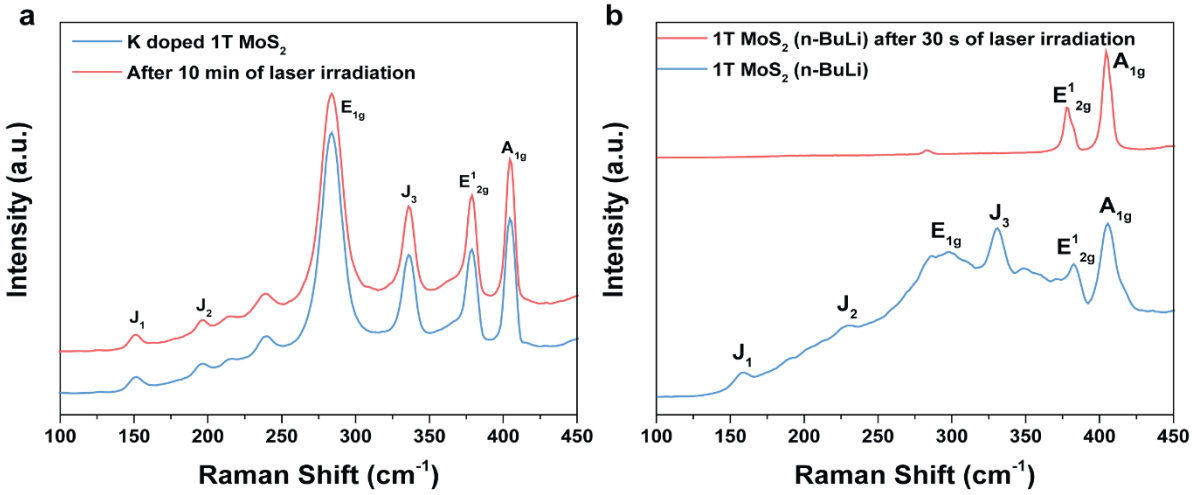

Figure 1.15. Raman spectra of (a) K doped 1T MoS_2 and (b) 1T MoS_2 (n-BuLi) after irradiation by a 532 nm laser source for 10 minute. When irradiated with a 532 nm laser, the 1T MoS_2 synthesized by n-BuLi is easily converted to the 2H phase.

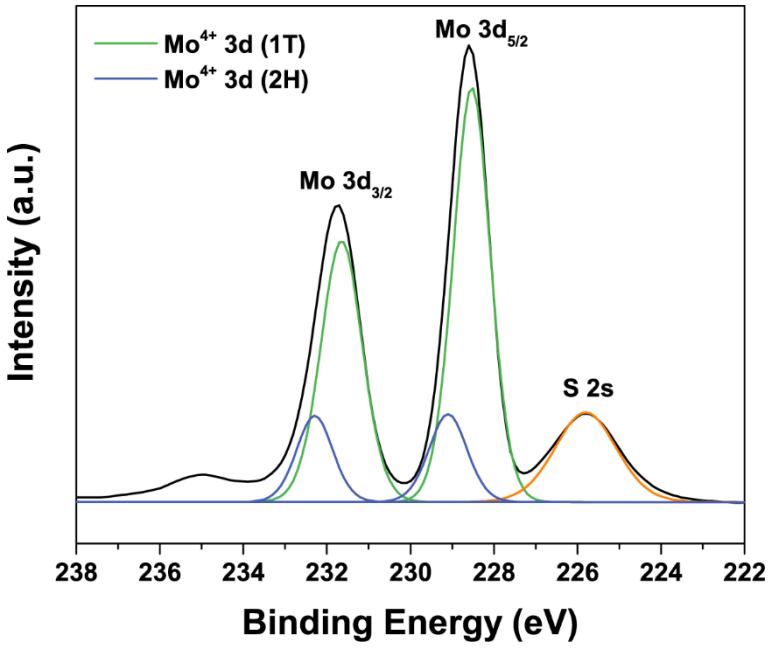

Figure 1.16. XPS spectra of 1T MoS_2 synthesized by using n-BuLi. The 1T phase ratio determined from the XPS results is ~ 75%.

1.7 Application of K doped 1T MoS_2 in electrocatalyst

Due to the unique structural and electrical characteristics, hydrophilicity characteristics and high content of 1T phase, K doped 1T MoS_2 heterostructure can be a potential electrocatalyst for hydrogen evolution reaction (HER). HER performance in acidic electrolytes is important, performance in alkaline electrolytes is also very important for simultaneous HER and oxygen evolution reactions (OER) in one cell. In order for HER to occur, an OER reaction must be preceded. Thus, there is a need for HER electrocatalysts that are effective in alkaline electrolytes. Thus, the electrocatalytic activity of K doped 1T MoS_2 was tested in 1 M KOH electrolyte as well as 0.5 M H_2SO_4 electrolyte. In addition, to confirm the relationship between high phase purity and HER performance of K doped 1T MoS_2, HER performance comparison with 1T MoS_2 (1T phase ratio ~75%, XPS result demonstrate in Figure 1.15) synthesized using n-BuLi was conducted. The HER activity was investigated by examing the rotating disk electrode (RDE) polarization curves. As shown in Figure1.17 a, d the HER performance and Tafel slope of K doped 1T MoS_2, 1T MoS_2 (n-BuLi) and 2H MoS_2 in acidic and alkaline electrolytes was compared. The overpotential at 10 mA cm^{-2} of K doped 1T MoS_2 is 222 mV and 253 mV in 0.5 M H_2SO_4 and 1 M KOH condition, respectively. Whereas overpotential at 10 mA cm^{-2} of 1T MoS_2 (n-BuLi) (325 mV in 0.5 M H_2SO_4 and 384 mV in 1 M KOH) and 2H MoS_2 (433 mV in 0.5 M H_2SO_4 and 513 mV in 1 M KOH) have a higher potential, which means more electrical energy is needed to produce hydrogen. Electrochemically active metallic 1T phase transition, higher phase purity than 1T MoS_2 (n-BuLi) and hydrophilicity demonstrate the superior HER performance of K doped 1T MoS_2 compared to 2H MoS_2 and 1T MoS_2 (n-BuLi) in 0.5 M H_2SO_4 and 1 M KOH condition (Table 1.2). As shown in Figure 1.17 b and e, low Tafel slope of K doped 1T MoS_2 (47 mV dec^{-1} in 0.5 M H_2SO_4 and 67 mV dec^{-1} in 1 M KOH). These finding obviously indicates that K-doped 1T-MoS_2 follows Volmer-Heyrovsky HER mechanism with the rate-determining step of the electrochemical desorption (Heyrovsky reaction: $H_{ads} + H_3O^+ + e^- \rightarrow H_2 + H_2O$), while the other catalysts struggle with the rate-determining step of electrochemical adsorption (Volmer reaction: $H_3O^+ + e^- \rightarrow H_{ads} + H_2O$).[46] To better understand the electrocatalytic property of K-doped 1T MoS_2, electrochemical impedance spectroscopy (EIS) test was carried out in Figure 1.16 c, f. As shown in the Nyquist plot, the significant decrease of the charge transfer resistance (R_{ct}) is observed for K-doped 1T MoS_2 (3.16 Ω) compared to 1T MoS_2 (n-BuLi) (8.46 Ω) and 2H MoS_2 (~70 Ω) at the overpotential of 0.3 V in 0.5 M H_2SO_4. The R_{ct} is again confirmed in 1 M KOH for K-doped 1T-MoS_2 (3.66 Ω) compared to 1T MoS_2 (n-BuLi) (~50 Ω) and 2H MoS_2 (~240 Ω) at the overpotential of 0.3 V, demonstrating that the efficient HER activities of K-doped 1T MoS_2 for both in 0.5 M H_2SO_4 and 1 M KOH.

The HER activities of K-doped 1T MoS_2 were further studied in the alkaline media of 1 M KOH which means K doped 1T MoS_2 highly efficient charge transfer process due to high electrical conductivity with high 1T phase ratio. In order to evaluate the electrochemical activity of the

electrocatalyst, the electrochemical double layer capacitance (C_{dl}) obtained through cyclic voltammetry (CV) was compared (Figure 1.16 g, Figure 1.17). The C_{dl} of K doped 1T MoS_2 is 10.78 mF cm^{-2} which is higher than 1T MoS_2 (n-BuLi) (7.26 mF cm^{-2}) and 2H MoS_2 (5.61 mF cm^{-2}). This suggests that K doped 1T MoS_2 have abundant active sites due to the higher phase purity of 1T phase region than 1T MoS_2 (n-BuLi) and 2H MoS_2. In addition, K doped 1T MoS_2 was also confirmed to have excellent HER stability (Figure 1.16 h, i, inset: chronoamperometry analysis). After 5000 cycles of CV, there are no remarkable performance loss for K doped 1T MoS_2 with negligible increment in η10 by 2 mV and 8 mV in 0.5 M H_2SO_4 and 1 M KOH condition, respectively. At an overpotential (222 mV and 253 mV in 0.5 M H_2SO_4 and 1 M KOH condition, respectively) applied bias for RHE, the K doped 1T MoS_2 exhibits a stable current density of ~10 mA cm^{-2} for 100 hours. HER stability performance of K doped 1T MoS_2 is consistent with 1T phase stability. The HER stability results of K doped 1T MoS_2 suggest that HER performance stability is also improved because of high stability to maintain 1T phase.

Turnover frequency (TOF) and electrochemically active surface area (ECSA) methods are effective techniques to study the surface of electrocatalysts. As shown in Figure 1.18, the TOF profiles measured in the both acidic and alkaline solutions, the TOF values of K-doped 1T MoS_2, 1T MoS_2 (n-BuLi), 2H MoS_2, and Pt/C were investigated. For K-doped 1T MoS_2, the overpotentials to achieve TOF value of 1.0 H_2 s^{-1} was 0.25 and 0.29 V for 0.5 M H_2SO_4 and 1 M KOH, respectively. Notably, K-doped 1T MoS_2 presented far higher TOF value than 1T-MoS_2 (n-BuLi) with more than two-order difference in TOF value, clearly indicating that the high HER activities of K-doped 1T MoS_2.

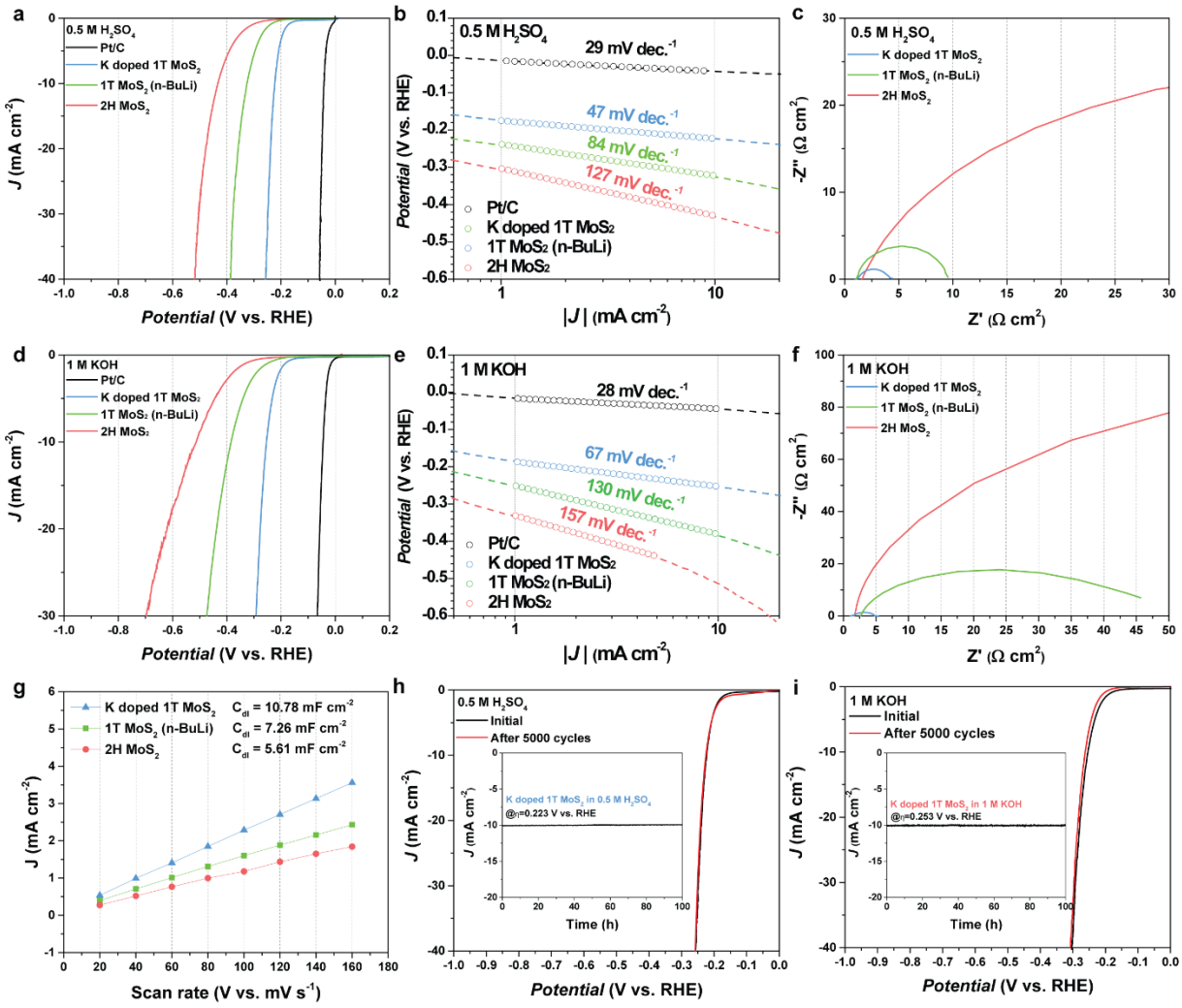

Figure 1.17. HER catalyst application (a, d) Linear sweep voltammetry (LSV) curves in (a) 0.5 M H_2SO_4 (d) 1 M KOH aqueous solution. (b, e) Corresponding Tafel slope for K doped 1T MoS_2, 1T MoS_2 (n-BuLi), 2H MoS_2, and Pt/C. (c, f) Electrochemical impedance spectroscopy of HER in (c) 0.5 M H_2SO_4 (f) 1 M KOH. (g) Electrochemical double layer capacitance of K doped 1T MoS_2, 1T MoS_2 (n-BuLi), and 2H MoS_2 obtained from CV. (h–i) CV cyclic stability profiles of K-doped 1T MoS_2 in (h) 0.5 M H_2SO_4, (i) 1 M KOH aqueous solution. Inset: Time dependent profiles of HER current density on K doped 1T MoS_2 at the overpotential.

	Overpotential in $0.5M\ H_2SO_4$ (-V, at 10 mA cm^{-2})	Overpotential in 1 M KOH (-V, at 10 mA cm^{-2})
K-doped 1T MoS_2	0.222	0.253
1T MoS_2 (n-BuLi)	0.325	0.384
2H MoS_2	0.433	0.513

Table 1.2. Comparison of HER overpotential of K-doped 1T MoS_2, 1T MoS_2 (n-BuLi), and 2H MoS_2 at 10 mA cm^{-2}.

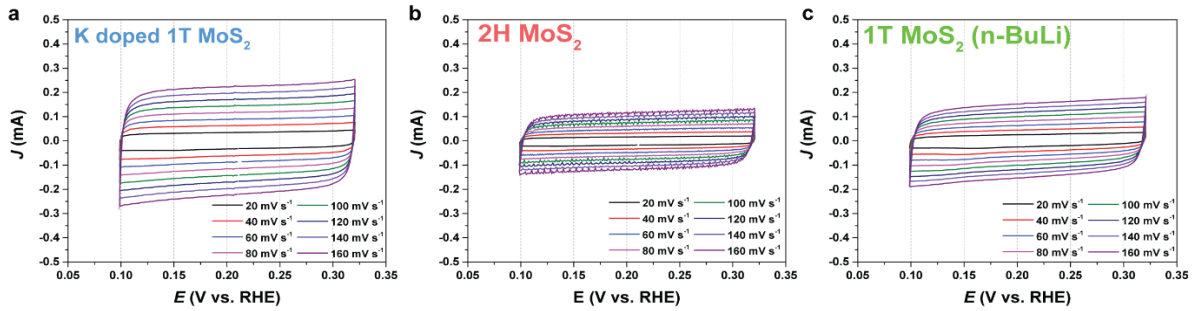

Figure 1.18. Cyclic voltammetric (CV) curves for (a) K doped 1T MoS_2, (b) 1T MoS_2 (n-BuLi), (c) 2H MoS_2

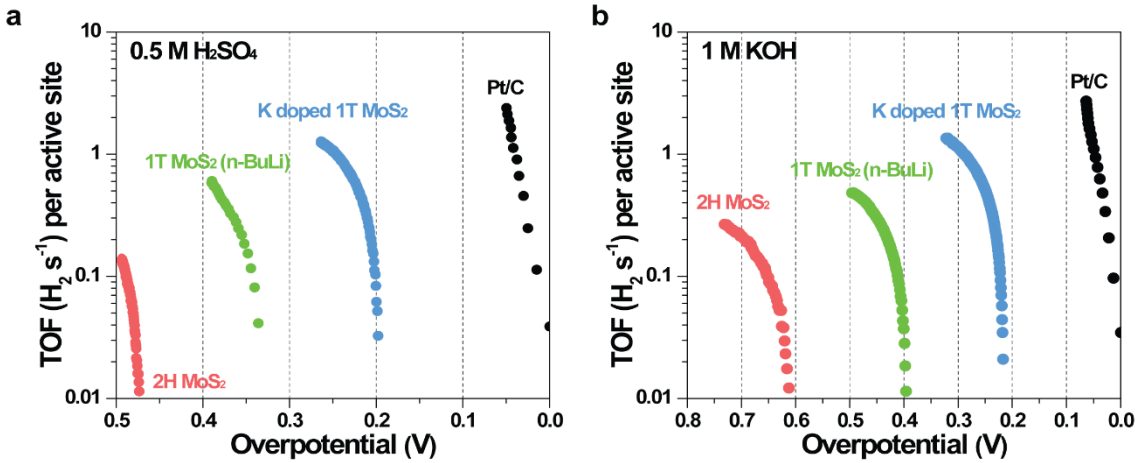

Figure 1.19. Turn over frequency (TOF) plots for the HER of K doped 1T MoS_2, 1T MoS_2 (n-BuLi), and 2H MoS_2.

1.8 Conclusion

The use of ionization potential gaps and capillary action between the highly reactive molten K metal and MoS_2 powder enabled the phase transition through efficient intercalation of MoS_2 interlayer K metal ion. The highly reactive molten K is not only intercalated between MoS_2 layers, but also doped into the lattice of MoS_2 to phase transition from 2H to 1T, as well as improving 1T phase stability through continuous electron transfer from K ion to MoS_2. As a result, K-doped 1T-MoS_2 also showed high 1T phase stability despite annealing at 350 ℃, air exposure for 300 days, and 532 nm Raman laser irradiation. K-doped 1T-MoS_2 also exhibits significantly improved electrical conductivity, high 1T phase purity, and hydrophilic properties. As a result, K-doped 1T-MoS_2 showed low overpotential (222 mV and 253 mV in 0.5 M H_2SO_4 and 1 M KOH condition, respectively), Tafel slope (47 mV dec^{-1} in 0.5 M H_2SO_4 and 67 mV dec^{-1} in 1 M KOH), R_{ct} value (3.16 Ω in 0.5 M H_2SO_4 and 3.66 Ω in 1 M KOH), and high electrochemical double layer capacitance (10.78 mF cm^{-2}) under acid and alkaline conditions. In addition, K-doped 1T-MoS_2 has stable performance for 5000 CV cycles and 100 hours due to high 1T phase stability and 1T phase-purity. These results suggest an effective and distinctive phase engineering method for TMDs and scalable synthesis method of 1T phase TMDs is provided.

2. References

(1) Kuc. A. Low-dimensional transition-metal dichalcogenides. *Chem Modell,* **2014,** 11, 1-29.

(2) Voiry. D.; Mohite. A.; Chhowalla. M. Phase engineering of transition metal dichalcogenides. *Chem. Soc. Rev.* **2015**, 44, 2702–2712.

(3) Mak, K. F.; Lee. C.; Hone. J.;, Shan. J.; Heinz. T. F. Atomically Thin MoS_2 : A New Direct-Gap Semiconductor. *Phys. Rev.Lett.* **2010**, 105, 136805.

(4) B¨oker. T.; Severin. R.; M¨uller. A.; Janowitz. C.; Manzke. R.; Voß. D.; Kr¨uger P.; Mazur. A.; Pollmann. J.; Band structure of MoS_2, $MoSe_2$, and α−$MoTe_2$: Angle-resolved photoelectron spectroscopy and ab initio calculations. *Phys. Rev. B: Condens. Matter Mater. Phys.* **2001**, 64, 235305.

(5) Chhowalla. M.; Shin H. S.; Eda G.; Li. L.-J.; Loh K. P.; Zhang H. The chemistry of two-dimensional layered transition metal dichalcogenide nanosheets, *Nat. Chem.* **2013**, 5, 263.

(6) Acerce. M.; Voiry. D.; Chhowalla. M. Metallic 1T phase MoS_2 nanosheets as supercapacitor electrode materials. *Nat. Nanotechnol.* **2015**, 10, 313–318.

(7) Lukowski. M. A.; Daniel. A. S.; Meng. F.; Forticaux. A.; Li. L. S.; Jin. S. Enhanced Hydrogen Evolution Catalysis from Chemically Exfoliated Metallic MoS_2 Nanosheets. *J. Am. Chem. Soc.* **2013**, 135, 10274–10277.

(8) Xu. J.; Zhang. J.; Zhang. W.; Lee. C. S. Interlayer Nanoarchitectonics of Two-Dimensional Transition-Metal Dichalcogenides Nanosheets for Energy Storage and Conversion Applications. *Adv. Energy Mater.* **2017**, 7, 1700571.

(9) Xu. B.; Wang. L.; Chen. H. J.; Zhao. J.; Liu. G.; Wu. M. S. Adsorption and diffusion of lithium on 1T-MoS_2 monolayer. *Comput. Mater. Sci.* **2014**, 93, 86–90.

(10) Jeong. Y. C.; Kim. J. H.; Kwon. S. H.; Oh. J. Y.; Park J.; Jung Y.; Lee S. G.; Yang S. J.; Park. C. R. Rational design of exfoliated 1T MoS2@CNT-based bifunctional separators for lithium sulfur batteries. *J. Mater. Chem. A.* **2017**, 5, 23909–23918.

(11) Aurbach. D.; Lu. Z.; Schechter. A.; Gofer. Y.; Gizbar. H.; Turgeman. R.; Cohen. Y.; Moshkovich. M.; Levi. E. Prototype systems for rechargeable magnesium batteries. *Nature*, **2000**, 407, 724.

(12) He. Z.; Que. W. Molybdenum disulfide nanomaterials: Structures, properties, synthesis and recent progress on hydrogen evolution reaction. *Appl. Mater. Today.* **2016**, 3, 23–56.

(13) Wang. H. T.; Lu. Z. Y.; Kong. D. S.; Sun. J.; Hymel. T. M.; Cui. Y. Electrochemical Tuning of MoS_2 Nanoparticles on Three-Dimensional Substrate for Efficient Hydrogen Evolution. *ACS Nano*, **2014**, 8, 4940–4947.

(14) Voiry. D.; Salehi. M.; Silva. R.; Fujita. T.; Chen. M. W.; Asefa T.; Shenoy. V. B.; Eda. G.; Chhowalla. M. Conducting MoS_2 Nanosheets as Catalysts for Hydrogen Evolution Reaction. *Nano Lett.* **2013**, 13, 6222–6227.

(15) Jiao. Y.; Mukhopadhyay. A.; Ma. Y.; Yang. L.; Hafez. A. M.; Zhu. H.; Lithium-Ion Batteries: Ion Transport Nanotube Assembled with Vertically Aligned Metallic MoS_2 for High Rate Lithium-Ion Batteries. *Adv. Energy Mater.* **2018**, 15, 1702779.

(16) Yin. Y.; Han. J.; Zhang. Y.; Zhang. X.; Xu. P.; Yuan. Q.; Samad. L.; Wang. X.; Wang. Y.; Zhang. Z.; Zhang. P.; Cao. X.; Song. B.; Jin. S. Contributions of Phase, Sulfur Vacancies, and Edges to the Hydrogen Evolution Reaction Catalytic Activity of Porous Molybdenum Disulfide Nanosheets. *J. Am. Chem. Soc.* **2016**, 138, 7965–7972.

(17) Mishra. R. K.; Manivannan. S.; Kim. K.; Kwon. H.-I.; Jin. S. H. Petal-like MoS_2 nanostructures with metallic 1 T phase for high performance supercapacitors. *Curr. Appl. Phys.* **2018**, 18, 345–352.

(18) Geng. X.; Zhang. Y.; Han. Y.; Li. J.; Yang. L.; Benamara. M.; Chen. L.; Zhu. H. Two-Dimensional Water-Coupled Metallic MoS_2 with Nanochannels for Ultrafast Supercapacitors. *Nano Lett.* **2017**, 17, 1825–1832.

(19) Segi. B.; Min. S. D.; Jin. Y.; Joon. Y. J. High-Power Supercapacitive Properties of Graphene Oxide Hybrid Films with Highly Conductive Molybdenum Disulfide Nanosheets. *ChemElectroChem.* **2015**, 2, 1938–1946.

(20) Li. X.; Qian. T.; Zai. J.; He. K.; Feng. Z.; Qian. X. Co stabilized metallic 1Td MoS2 monolayers: Bottom-up synthesis and enhanced capacitance with ultra-long cycling stability. *Mater. Today Energy*. **2018**, 7, 10–17.

(21) Eda. G.; Yamaguchi. H.; Voiry. D.; Fujita. T.; Chen. M.; Chhowalla. M. Photoluminescence from Chemically Exfoliated MoS_2. *Nano Lett.* **2011**, 11, 5111–5116.

(22) Nurdiwijayanto. L.; Ma. R.; Sakai. N.; Sasaki. T. Stability and Nature of Chemically Exfoliated MoS_2 in Aqueous Suspensions. *Inorg. Chem.* **2017**, 56, 7620–7623.

(23) Kappera. R.; Voiry. D.; Yalcin. S. E.; Jen. W.; Acerce. M.; Torrel. S.; Branch. B.; Lei. S. D.; Chen. W. B.; Najmaei. S.; Lou. J.; Ajayan. P. M.; Gupta. G.; Mohite. A. D.; Chhowalla. M. Metallic 1T phase source/drain electrodes for field effect transistors from chemical vapor deposited MoS_2. *APL Mater.* **2014**, 2, 6.

(24) Li. Y.; Wang. L. L.; Zhang. S. Q.; Dong. X. R.; Song. Y. Z.; Cai. T.; Liu. Y. T. Cracked monolayer 1T MoS_2 with abundant active sites for enhanced electrocatalytic hydrogen evolution. *Catal. Sci. Technol.* **2017**, 7, 718–724.

(25) Liu. Q.; Li. X.; Xiao. Z.; Zhou. Y.; Chen. H.; Khalil. A.; Xiang. T.; Xu. J.; Chu. W.; Wu. X.; Yang. J.; Wang. C.; Xiong. Y.; Jin. C.; Ajayan. P. M.; Song. L. Stable Metallic 1T-WS_2 Nanoribbons Intercalated with Ammonia Ions: The Correlation between Structure and Electrical/Optical Properties. *Adv. Mater.* **2015**, 27, 4837–4844

(26) Wang. S.; Zhang D.; Zhang. C.; Du. Z.; Yin. H.; Bi X.; Yang. S. Ultrastable In-Plane 1T–2H

MoS_2 Heterostructures for Enhanced Hydrogen Evolution Reaction. *Adv. Energy Mater.* **2018**, 8, 1801345.

(27) Acrivos. J. V.; Liang. W. Y.; Wilson. J. A.; Yoffe. A. D. Optical studies of metal-semiconductor transmutations produced by intercalation. *J. Phys. C: Solid State Phys.* **1971**, 4, L18.

(28) Conley. H. J.; Wang. B.; Ziegler. J. I.; Haglund. R. F.; Pantelides. S. T.; Bolotin. K. I. Bandgap Engineering of Strained Monolayer and Bilayer MoS_2. *Nano Lett.* **2013**, 13, 3626–3630.

(29) Hui. Y. Y.; Liu. X.; Jie. W.; Chan. N. Y.; Hao. J.; Hsu. Y.-T.; Li. L.-J.; Guo. W. ; Lau. S. P. Exceptional Tunability of Band Energy in a Compressively Strained Trilayer MoS_2 Sheet. *ACS Nano.* **2013**, 7, 7126–7131.

(30) Liu. Y. Y.; Xie. Y.; Liu. L. J.; Jiao. J. L. Sulfur vacancy induced high performance for photocatalytic H_2 production over 1T@2H phase MoS_2 nanolayers. *Catal. Sci. Technol.* **2017**, 7, 5635–5643.

(31) Liu. Q.; Li. X.; He. Q.; Khalil. A.; Liu. D.; Xiang. T.; Wu. X.; Song. L. Gram-Scale Aqueous Synthesis of Stable Few-Layered 1T-MoS2 : Applications for Visible-Light- Driven Photocatalytic Hydrogen Evolution. *Small*, **2015**, 11, , 5556–5564.

(32) X. B. Fan,; P. T. Xu,; D. K. Zhou,; Y. F. Sun,; Y. G. C. Li,; M. A. T. Nguyen,; M. Terrones,;, T. E. Mallouk. Fast and Efficient Preparation of Exfoliated 2H MoS_2 Nanosheets by Sonication-Assisted Lithium Intercalation and Infrared Laser-Induced 1T to 2H Phase Reversion. *Nano Lett.* **2015**, 15, 5956.

(33) R. Y. Zhang.; I. L. Tsai.; J. Chapman.; E. Khestanova.; J. Waters.; I. V. Grigorieva. Superconductivity in Potassium-Doped Metallic Polymorphs of MoS_2. *Nano Lett.* **2016**, 16, 629.

(34) S. Bo.; Cui. X.; Jiao. L.; Qi. K.; Wang. Y.; Fan. J.; Yue. Y.; Wang. H.; Bao. Q.; Fan. X.; Wei. X.; Song. W.; Cheng.; Guo. S.; Zheng. W.; Lattice -Mismatch-Induced Ultrastable 1T-Phase MoS_2−Pd/Au for Plasmon-Enhanced Hydrogen Evolution. *Nano Lett.* **2019**, 19, 2758−2764

(35) Liu. L.; Wu. J.; Wu. L.; Ye. M.; Liu. X.; Wang. Q.; Hou. S.; Lu. P.; Sun. L.; Zheng. J.; Xing. L.; Gu. L.; Jiang. X.; Xie. L.; Jiao. L. Phase-selective synthesis of 1T' MoS_2 monolayers and heterophase bilayers. *Nat. Chem.* **2018**, 10, 638-643

(36) Voiry. D.; Fullon. R.; Yang. J.; de Carvalho Castro E Silva. C.; Kappera. R.; Bozkurt. I.; Kaplan. D.; Lagos. MJ.; Batson. P. E.; Gupta. G.; Mohite. A. D.; Dong. L.; Er. D.; Shenoy. V. B.; Asefa. T.; Chhowalla. M. The role of electronic coupling between substrate and 2D MoS_2 nanosheets in electrocatalytic production of hydrogen. *Nat. Mater.* **2016**, 15, 1003-1009.

(37) Uraban. F.; Passacantando. M.; Giubileo. F.; Iemmo. L.; Bartolomeo D. B. Transport and Field Emission Properties of MoS_2 Bilayers. *Nanomaterials*, **2018**, 8, 151.

(38) Park. K. H.; Lee. D.; Kim. J.; Song. J.; Lee. Y. M.; Kim H. T.; Park. J. K. Defect-Free, Size Tunable Graphene for High-Performance Lithium Ion Battery. *Nano Lett.* **2014**, 14, 4306-4313.

(39) Zheng. J.; Zhang H.; Dong. S.; Liu. Y.; Nai. C. T.; Shin. H. S.; Jeong. H. Y.; Liu. B.; Loh K. P. High yield exfoliation of two-dimensional chalcogenides using sodium naphthalenide. *Nat. Comm.* **2014**, 5, 2995.

(40) Jauncey. G. E. M., The Scattering of X-Rays and Bragg's Law. *Proc Natl Acad Sci U S A.* **1924** 10, 57–60.

(41) S. Jimenez. Sandoval.; D. Yang.; R. F. Frindt.; J. C. Irwin.; Raman study and lattice dynamics of single molecular layers of MoS_2. *Phys. Rev. B*, **1991**, 44, 3955.

(42) Lin. Y.-C.; Dumcencon. D. O.; Huang. Y.-S.; Suenaga. K. Atomic mechanism of the semiconducting-to-metallic phase transition in single-layered MoS_2. *Nat. Nanotechnol.* **2014**, 9, 391–396.

(43) Leng. K.; Chen. Z.; Zhao. X.; Tang. X.; Tang. W.; Tian. B.; Nai. C. T.; Zhou. W.; Loh. K. P. Phase Restructuring in Transition Metal Dichalcogenides for Highly Stable Energy Storage. *ACS Nano*, **2016**, 10, 9208−9215.

(44) Ma. F. X.; Gao. G. P.; Jiao. Y. L.; Gu. Y. T.; Bilic. A.; Zhang. H. J.; Chen. Z. F.; Du A. J. Predicting a new phase (T″) of two-dimensional transition metal di-chalcogenides and strain-controlled topological phase transition. *Nanoscale*, **2016**, 8, 4969.

(45) Yu. Y.; Nam. G. H.; He. Q.; Wu. X. J.; Zhang. K.; Yang. Z.; Chen. J.; Ma. Q.; Zhao. M.; Liu. Z.; Ran. F. R.; Wang. X.; Li. H.; Huang. X.; Li. B.; Xiong. Q.; Zhang. Q.; Liu. Z.; Gu. L.; Du. Y.; Huang. W.; Zhang. H. High phase-purity 1T'-MoS_2- and 1T'-$MoSe_2$-layered crystals. *Nat. Chem.* **2018**, 10, 638-643.

(46) M.R. Gennero de Chialvo.; A. C. Chialvo. Kinetics of hydrogen evolution reaction with Frumkin adsorption: re-examination of the Volmer–Heyrovsky and Volmer–Tafel routes. *Electrochimica Acta*, **1998**, 44, 841-851.

Acknowledgement

First, I would like to express my gratitude to my advisor professor Hyesung Park for sincere advising and support of my research and study during master's course. Thanks to his guidance, I achieved my research results and completed master's degree. Also, I thank to professor Jungki Ryu and Jun Hee Lee for advising the detailed feedbacks and specific advice of thesis and research topic.

I thanks to LEC lab member who help me and work together, especially Nam Khen Oh, Junghyun Lee, Ungsoo Kim, Jihyung Seo, who characterized XPS, AFM and TEM images of K-doped 1T-MoS_2, electrical conductivity, and water contatct angle. I also thank to Guntea Kim's group for electrocatalyst experiment.